

# Molecules in Real Cavities with Quantum Electrodynamical Density Functional Theory

Mark Kamper Svendsen,<sup>1,2,3,\*</sup> Kristian Sommer Thygesen,<sup>2</sup> Angel Rubio,<sup>1,3,4</sup> and Johannes Flick<sup>3,5,6</sup>

<sup>1</sup>*Max Planck Institute for the Structure and Dynamics of Matter and  
Center for Free-Electron Laser Science & Department of Physics,  
Luruper Chaussee 149, 22761 Hamburg, Germany*

<sup>2</sup>*CAMD, Department of Physics, Technical University of Denmark, 2800 Kgs. Lyngby, Denmark*

<sup>3</sup>*Center for Computational Quantum Physics, Flatiron Institute, New York, New York 10010, USA*

<sup>4</sup>*Nano-Bio Spectroscopy Group and European Theoretical Spectroscopy Facility (ETSF),  
Universidad del País Vasco (UPV/EHU), Av. Tolosa 72, 20018 San Sebastian, Spain*

<sup>5</sup>*Department of Physics, City College of New York, New York, New York 10031, USA*

<sup>6</sup>*Department of Physics, The Graduate Center, City University of New York, New York, New York 10016, USA*

(Dated: May , 2023)

Rapid experimental progress in realizing strongly coupled light-matter systems in complex electromagnetic environments necessitates the development of theoretical methods capable of treating light and matter from first principles. A popular such method is quantum electrodynamical density functional theory (QEDFT) which is a generalization of density functional theory to situations where the electronic system is coupled to quantized light modes. While this method provides a powerful description of the electronic system and the quantized modes of light, it has so far been unable to deal correctly with absorbing and dispersing electromagnetic media in practice. In addition, the cavity field strength parameters have not been linked to the real electromagnetic environment in which the matter is embedded meaning that these are effectively free parameters. In this paper, we discuss how macroscopic QED (MQED) can be invoked to correctly parameterize QEDFT for realistic optical cavity setups. To exemplify this approach, we consider the example of an absorbing spherical cavity and study the impact of different parameters of both the environment and the electronic system on the transition from weak-to-strong coupling. As a result of our work, the coupling parameters in general, lossy environments can be now expressed in terms of the *classical* Dyadic Green's Function. Because the Dyadic Green's Function is completely determined by the electromagnetic environment and the boundary conditions, it thus removes the light-matter coupling strengths as free parameters. As part of this work, we also provide an easy to use tool that can calculate the cavity coupling strengths for simple cavity setups.

## INTRODUCTION

Recent years have seen rapid developments in the experimental realization of novel setups, where light and matter are strongly coupled. Examples include plasmonic nanocavities [1], optical cavities using four-wave mixing schemes [2], metasurface systems [3], self-assembled Casimir microcavities [4], deep-strong coupling in plasmonic nanoparticles [5], and many more [6, 7]. Due to the inherent complexity of these general strongly coupled light-matter systems, theoretical methods usually apply various simplifications to keep simulations tractable. One first-principles method which has gained popularity is the recently introduced quantum-electrodynamical density-functional theory (QEDFT) [8]. QEDFT is a generalization of density-functional theory (DFT) [9] for electronic systems interacting strongly with quantized modes of the electromagnetic field. The method represents a good compromise between accuracy and computational cost, and it has been successfully applied to describe both the ground-state [10, 11], and excited-states [12, 13] of single (few) molecules strongly coupled to quantized modes of light, as well as for applications in polaritonic chemistry [14].

The existence of the QEDFT formulation can be proven under very general conditions [8] and it in prin-

ciple allows for the treatment of coupled light-matter systems with many electrons and many photonic modes under very general conditions. However, currently, most practical implementations of QEDFT are based on the dipole approximation for the light-matter coupling, and a discrete mode expansion of the electromagnetic field. The latter implies that the material or molecular system of interest is embedded in a lossless electromagnetic medium. There have been previous studies at applying the QEDFT formulation to lossy optical cavities to describe e.g. photon losses through cavity mirrors [12, 15, 16]. Here, different models of the optical cavity were used, but no general connection between the cavity field parameters and the optical environment for absorbing and dispersing magnetoelectric bodies has yet been established. As a result, the electron-photon coupling parameters, while in principle connected to the physical quantity of the vacuum electric field at the center of charge of the system, are then in practice often treated as free parameters. This highlights the other current practical limitation of QEDFT: Treating the cavity coupling parameters as essentially free parameters makes quantitative calculations and direct comparison with experiments hard.

In the presence of absorbing and dispersing magnetoelectric bodies in the electromagnetic environments, it

is not possible to correctly quantize the electromagnetic field via discrete modes. Instead, the field quantization can be realized as a continuous expansion using the *classical* dyadic Green's function (DGF) in the framework of macroscopic quantum electrodynamics (MQED) [17]. It has previously been shown how standard DFT can be combined with MQED to provide a quantitative, first principles description of the quantum light-matter interactions for real cavity setups in the weak and intermediate coupling regimes beyond the dipole approximation [18]. However, the previous work relied on a wave function ansatz which only considered a subset of the electronic structure. This is expected to become problematic in the ultra- and deep strong coupling regimes.

In this work, we overcome the shortcomings of the existing methodologies by establishing a direct connection between the frameworks of MQED and QEDFT that can be used to study the interaction of molecular systems with arbitrary quantized electromagnetic fields while correctly considering absorbing and dispersing electromagnetic environments. Specifically, we investigate how QEDFT can be formulated in terms of the field expansion from MQED within the dipole approximation for the light matter coupling. This in turn allows us to express the cavity coupling parameters in terms of the *classical* DGF, which can be related to a real cavity setup. The result is that we arrive at a formulation of QEDFT appropriate in lossy electromagnetic environments which simultaneously relates the coupling parameters to a real cavity. This removes the electron-photon coupling strengths as free parameters. We will exemplify this scheme on a lossy spherical microcavity setup and study the impact of different parameters of both the environment and the electronic system on the transition from weak-to-strong coupling.

### EMITTER-CENTERED FORMULATION OF MACROSCOPIC QUANTUM ELECTRODYNAMICS

Macroscopic Quantum Electrodynamics (MQED) is a framework for quantizing the electromagnetic field in the presence of arbitrary absorbing or dispersing environments [17–19]. The central object in MQED is the *classical* Green's function that solves the Helmholtz equation for a point source, the so-called dyadic Green's function (DGF) [20],

$$\left[ \nabla \times \kappa(\mathbf{r}, \omega) \nabla \times - \frac{\omega^2}{c^2} \epsilon(\mathbf{r}, \omega) \right] \mathbf{G}(\mathbf{r}, \mathbf{r}', \omega) = \delta(\mathbf{r} - \mathbf{r}'), \quad (1)$$

where  $\kappa(\mathbf{r}, \omega) = \mu^{-1}(\mathbf{r}, \omega)$  and  $\epsilon(\mathbf{r}, \omega)$  are the spatially dependent dielectric function and inverse magnetic permeability respectively. The DGF is of central importance to the quantized theory of electromagnetic fields in lossy

environments because it simultaneously carries the information about the electromagnetic boundary conditions, and serves as a projector from the coupled light-matter system onto the electromagnetic degrees of freedom [17].

For a spatially local magnetoelectric medium in the nonrelativistic limit, the MQED expansion of the electric field in the Power-Zienau-Woolley (PZW) frame [21, 22] (multipolar gauge) can be written as [17, 19],

$$\hat{\mathbf{E}}(\mathbf{r}) = \int d\omega \hat{\mathbf{E}}(\mathbf{r}, \omega) + \text{h.c.}, \quad (2)$$

$$\hat{\mathbf{E}}(\mathbf{r}, \omega) = \sum_{\lambda=e,m} \int d^3r' \mathbf{G}_\lambda(\mathbf{r}, \mathbf{r}', \omega) \cdot \hat{\mathbf{f}}_\lambda(\mathbf{r}', \omega). \quad (3)$$

Here  $\hat{\mathbf{f}}_\lambda(\mathbf{r}', \omega)$  are the spatially resolved polaritonic field operators of MQED which fulfill the commutation relations of the quantum harmonic oscillator, and  $\mathbf{G}_e(\mathbf{r}, \mathbf{r}', \omega)$  and  $\mathbf{G}_m(\mathbf{r}, \mathbf{r}', \omega)$  are the electric and magnetic components of the DGF respectively,

$$\mathbf{G}_e(\mathbf{r}, \mathbf{r}', \omega) = i \frac{\omega^2}{c^2} \sqrt{\frac{\hbar}{\pi \epsilon_0} \text{Im} \epsilon(\mathbf{r}, \omega)} \mathbf{G}(\mathbf{r}, \mathbf{r}', \omega), \quad (4)$$

$$\mathbf{G}_m(\mathbf{r}, \mathbf{r}', \omega) = -i \frac{\omega}{c} \sqrt{\frac{\hbar}{\pi \epsilon_0} \text{Im} \mu(\mathbf{r}, \omega)} \mathbf{G}(\mathbf{r}, \mathbf{r}', \omega) \times \nabla'. \quad (5)$$

In the following we neglect magnetic interactions and consider the coupling between light and matter within the dipole approximation. Therefore, if we consider a set of emitters  $i$  with positions (centers of charge)  $\mathbf{r}_i$ , the interaction only samples the electromagnetic field at these positions. In this sense, the full electric field  $\hat{\mathbf{E}}(\mathbf{r})$  in Eq. 2 contains more information than strictly necessary to describe the light-matter interaction completely. As discussed in Refs [19, 23, 24], it is therefore possible to arrive at a significantly more compact expression by alternatively expanding the electric field in terms of a set of  $\mathcal{N}$  explicitly orthogonalized bright modes at each frequency,

$$\hat{\mathbf{E}}(\mathbf{r}) = \sum_{i=1}^{\mathcal{N}} \int_0^\infty d\omega \mathbf{E}_i(\mathbf{r}, \omega) \hat{C}_i(\omega) + \text{H.c.}, \quad (6)$$

$$\mathbf{E}_i(\mathbf{r}, \omega) = \frac{\hbar \omega^2}{\pi \epsilon_0 c^2} \sum_{j=1}^{\mathcal{N}} V_{ij}^*(\omega) \frac{\text{Im} \mathbf{G}(\mathbf{r}, \mathbf{r}_j, \omega) \cdot \hat{\mathbf{n}}_j}{G_j(\omega)}. \quad (7)$$

Here  $\hat{C}_i^{(\dagger)}(\omega)$  destroys (creates) a photon in the  $i$ th bright mode.  $\mathbf{E}_i(\mathbf{r}, \omega)$  describes the spatial mode function of the electric field associated with mode  $i$ . The normalisation factor  $G_j(\omega)$  is the square root of the dipole spectral density [25],

$$G_j(\omega) = \left( \frac{\hbar \omega^2}{\pi \epsilon_0 c^2} \mathbf{n}_j \cdot \text{Im} \mathbf{G}(\mathbf{r}_j, \mathbf{r}_j, \omega) \cdot \mathbf{n}_j \right)^{1/2}. \quad (8)$$

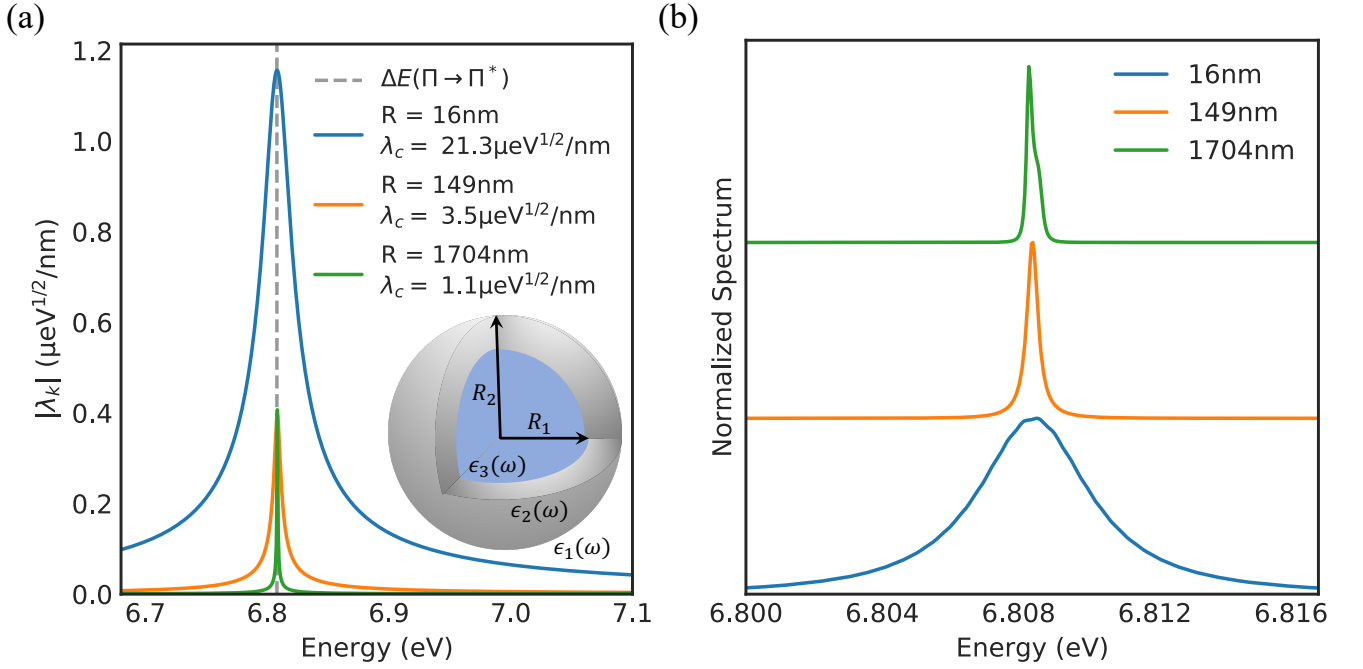


**FIG. 1.** (a) Different radii of the spherical microcavity that host a resonance that aligns with the  $\Pi \rightarrow \Pi^*$  of the benzene molecule. The total light-matter coupling strength of the modes is also shown in the legend, and it can be clearly observed that the cavity-coupling strength grows with decreasing cavity radius. The mode structure is shown with a sampling density of 10 points/meV. (b) The linear absorption spectrum of benzene as a function of cavity radius showing a clear radius dependent Purcell enhancement.

Finally, the matrix  $V_{ij}(\omega)$  is the transformation matrix which obeys  $\mathbf{V}(\omega)\mathbf{S}(\omega)\mathbf{V}^\dagger(\omega) = \mathbf{I}$  where

$$S_{ij}(\omega) = \frac{\hbar\omega^2}{\pi\epsilon_0c^2} \frac{\mathbf{n}_i \cdot \text{Im}\mathbf{G}(\mathbf{r}_i, \mathbf{r}_j, \omega) \cdot \mathbf{n}_j}{G_i(\omega)G_j(\omega)}, \quad (9)$$

and it is a result of the mode-orthogonalization inherent to the emitter-centered representation [19]. The number of emitter centered modes per frequency,  $\mathcal{N}$ , is equal to the number of emitter positions times the number of dipole orientations considered. In this work, we consider a single emitter position  $\mathbf{r}_0$  and the full three-dimensional space of dipole orientations. This results in three emitter-centered modes per frequency.

We want to express the total Hamiltonian of the coupled light-matter system in a similar form as used previously in Refs. [12, 15, 26]. Therefore we write (see Supplementary note A),

$$\mathcal{H} = \mathcal{H}_{\text{Mat}} + \frac{1}{2} \sum_{i=1}^{\mathcal{N}} \int_0^\infty d\omega \left\{ \hat{p}_i(\omega)^2 + \omega^2 \left[ \hat{q}_i(\omega) + \frac{\lambda_i(\omega)}{\omega} \cdot \hat{\mathbf{R}} \right]^2 \right\}. \quad (10)$$

The light-matter interaction now contains the dipole moment operator for  $N_e$  electrons with position  $\hat{\mathbf{r}}_i$ ,  $\hat{\mathbf{R}} = \sum_{i=1}^{N_e} \hat{\mathbf{r}}_i$ , which gives rise to an explicit electron-photon interaction and the dipole-self energy term.  $\mathcal{H}_{\text{Mat}}$

is the standard matter Hamiltonian that describes the electronic system. The cavity field strength  $\lambda_i(\omega)$  is given by  $\lambda_i(\omega) = -e \left(\frac{2}{\hbar\omega}\right)^{1/2} \mathbf{E}_i(\mathbf{r}_0, \omega)$ , where  $\mathbf{r}_0$  denotes the center of charge. We have further introduced the photon field quantities  $\hat{p}_i$  and  $\hat{q}_i$  that are connected to the magnetic- and electric field in their corresponding mode and are given explicitly by  $\hat{q}_i(\omega) = \left(\frac{\hbar}{2\omega}\right)^{1/2} (\hat{C}_i(\omega) + \hat{C}_i^\dagger(\omega))$  and  $\hat{p}_i(\omega) = \left(\frac{\hbar\omega}{2}\right)^{1/2} (\hat{C}_i(\omega) - \hat{C}_i^\dagger(\omega))$ . In terms of these new quantities, the electric field expansion at the center of charge  $\mathbf{r}_0$  reads,

$$\hat{\mathbf{E}}(\mathbf{r}_0) = - \sum_{i=1}^{\mathcal{N}} \int_0^\infty \omega \lambda_i(\omega) \hat{q}_i(\omega) d\omega. \quad (11)$$

The interaction of the electronic system with the electric field within the dipole approximation can thus be expressed as the interaction of the electronic system and a continuous set of quantum harmonic oscillator modes via the dipole moment of the electronic system. Note that this formulation addresses both the problem of how to formulate the length gauge Hamiltonian in the presence of losses, and allows for the explicit calculation of the cavity field strengths in terms of the boundary conditions set by the cavity via the DGF of the electromagnetic field.

## QUANTUM ELECTRODYNAMIC DENSITY FUNCTIONAL THEORY

To calculate the excited-state properties of the coupled electron-photon problem defined by the Hamiltonian in Eq. 10, we employ the linear response formulation of QEDFT, which has been described in detail in Refs. [12, 13, 27]. Importantly, this method considers the *full* electronic structure of the matter system and goes beyond the rotating wave approximation. By combining it with the MQED quantization of the electromagnetic field we thus go beyond the method presented in Ref. [18]. Specifically, we employ the generalized Casida formulation of linear response QEDFT to calculate the oscillator strengths of the many-body excitations of the coupled light-matter (polaritonic) system. The generalized Casida equation reads,

$$\begin{bmatrix} U & V \\ V^T & \omega_\alpha \end{bmatrix} \begin{bmatrix} \mathbf{F} \\ \mathbf{P} \end{bmatrix} = \Omega_S^2 \begin{bmatrix} \mathbf{F} \\ \mathbf{P} \end{bmatrix}. \quad (12)$$

Here  $\omega_\alpha$  is a diagonal matrix with the frequency of photon modes in the diagonal.  $U$  accounts for the coupling between the electrons. Introducing the pair orbital index  $S = (ia)$ , corresponding to the pair orbital  $\Phi_S(\mathbf{r}) = \phi_i(\mathbf{r})\phi_a^*(\mathbf{r})$  with energy  $\epsilon_S = \epsilon_a - \epsilon_i$ ,  $U$  can be expanded as,

$$U_{SS'} = \epsilon_S^2 \delta_{SS'} + 2\epsilon_S^{1/2} K_{SS'}(\Omega_S) \epsilon_{S'}^{1/2}, \quad (13)$$

$$K_{SS'}(\Omega_S) = \int \int d\mathbf{r} d\mathbf{r}' \Phi_S(\mathbf{r}) f_{\text{Mxc}}^n(\mathbf{r}, \mathbf{r}', \Omega_S) \Phi_{S'}(\mathbf{r}'). \quad (14)$$

If  $N_{\text{pair}}$  pair-orbitals are included in the calculation,  $U$  is therefore an  $N_{\text{pair}} \times N_{\text{pair}}$  matrix.  $V_{\alpha S}$  is the matrix accounting for the coupling between the electrons and the photon modes,

$$V_{\alpha S} = 2\sqrt{\epsilon_S M_{\alpha S}(\Omega_S) N_{\alpha S} \omega_\alpha}, \quad (15)$$

$$M_{\alpha, S}(\Omega_S) = \int d\mathbf{r} \Phi_S(\mathbf{r}) f_{\text{Mxc}}^{q\alpha}(\mathbf{r}, \Omega_S), \quad (16)$$

$$N_{\alpha, S} = \frac{1}{2\omega_\alpha^2} \int d\mathbf{r} \Phi_S(\mathbf{r}) g_M^{q\alpha}(\mathbf{r}). \quad (17)$$

The size of these matrices will be  $N_{\text{photon}} \times N_{\text{pair}}$ . The  $\mathbf{F}$  part of the eigenvector in Eq. 12 can be interpreted as the matter part and the  $\mathbf{P}$  can be interpreted as the photon part. The square norm of the two gives the electronic- and photonic fraction of the excitation respectively. As discussed in Ref. [12] it is possible to calculate the oscillator strengths of the coupled system in terms of these eigenvectors. Finally, note that when neglecting the quantized light, only the top left block in Eq. 12 survives and one recovers the standard Casida formulation of linear response TDDFT for finite systems [28]. We note that these equations include the exchange correlation kernels  $f_{\text{Mxc}}^n$ ,  $f_{\text{Mxc}}^q$  and  $g_M^{q\alpha}$  which have to be

approximated in practice. So far the available exchange-correlation functionals for QEDFT in the time-domain are still limited [10, 11], but recent developments based on the photon-free formulation of QEDFT [29] or the QEDFT fluctuation-dissipation theorem [30] are promising. In this work, we neglect any exchange-correlation contribution in the kernels and apply the mean-field photonic random phase approximation. We refer to Ref. [12] for a thorough discussion of this approximation.

The excitation spectrum is then characterized by the strength function [12],

$$S(\omega) = \sum_I f_I \delta(\omega - \omega_I), \quad (18)$$

where  $f_I$  is the oscillator strengths, and  $I$  runs over the many-body excitations of the coupled light-matter (polaritonic) system. We emphasize that in this work we do not apply any broadening to the spectra and that the width of the peaks is determined completely by the electromagnetic environment. This highlights a further advantage of using the QEDFT-MQED combination, namely that this provides a natural description of the transition linewidths as they relate to decay induced by the electromagnetic environment. This is relevant beyond cavity QED settings and paves the way towards TDDFT without artificial linewidths.

## SPHERICAL MICROCAVITY

To exemplify the developed approach, we consider the spherically layered microcavity also considered in Ref. [31]. As shown in the inset of Fig. 1a, the spherical cavity consists of three concentric spherical layers, each characterized by a frequency dependent dielectric function,  $\epsilon_n(\omega)$ . In general, the source and field points ( $\mathbf{r}$  and  $\mathbf{r}'$ , respectively) can be in either the same layer or different layers. Consequently, the DGF for the reflected field is a nine-component object, where each of the components is a three-dimensional dyad. Labelling the possible combinations of source and field points by two extra indices  $m, n = 1, 2, 3$ , the full DGF of the system therefore takes the following form,

$$\mathbf{G}_{mn}(\mathbf{r}, \mathbf{r}', \omega) = \mathbf{G}^{\text{vac}}(\mathbf{r}, \mathbf{r}', \omega) \delta_{nm} + \mathbf{G}_{mn}^{\text{ref}}(\mathbf{r}, \mathbf{r}', \omega), \quad (19)$$

where  $\mathbf{G}^{\text{vac}}$  and  $\mathbf{G}^{\text{ref}}$  are the components of the DGF describing the free dipole field and the reflections of the dipole field in the surroundings, respectively. In combination, the two fully describe the electromagnetic environment of the cavity. Due to the spherical symmetry of the problem, the DGF of the system is most efficiently expanded onto vector spherical harmonics [20]. The nine different components of the reflection contribution can be calculated by explicitly invoking the electromagnetic

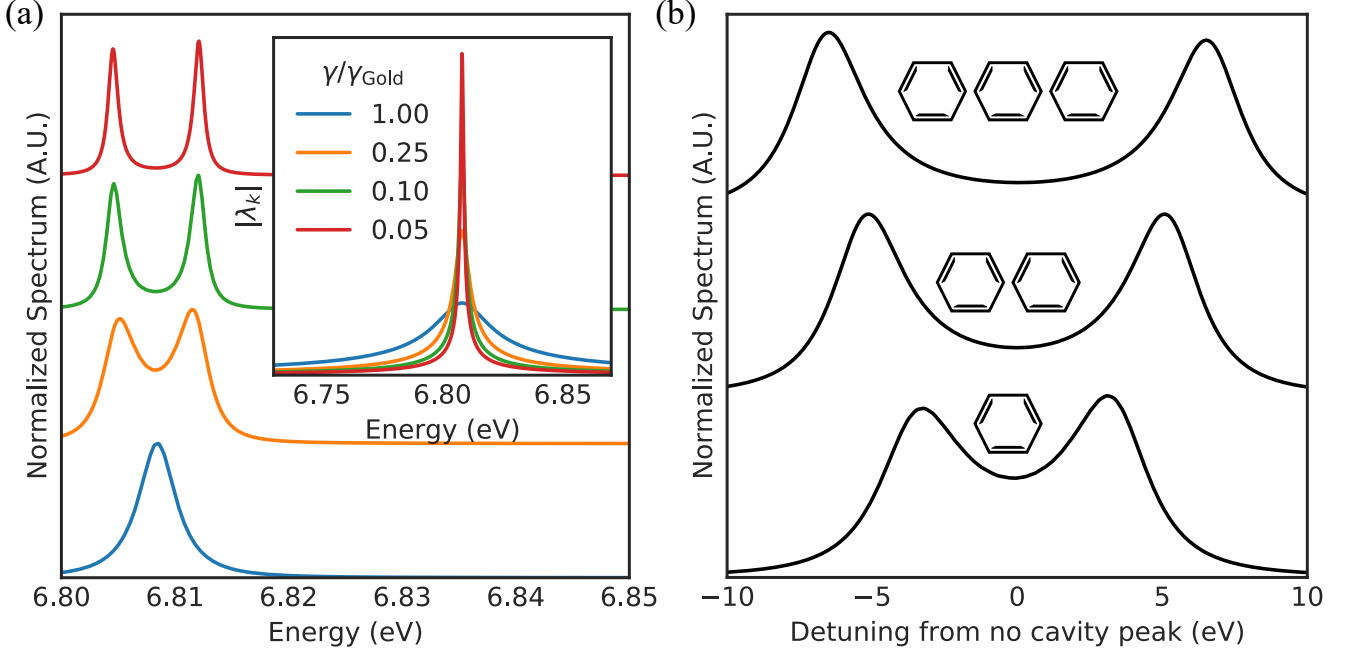


**FIG. 2.** (a) The linear absorption spectrum of benzene in the gold cavity from Fig. 1a with an inner radius  $R = 16\text{nm}$  as a function of the Drude damping in the metallic mirror region. (b) The linear absorption spectrum in a cavity with with an inner radius  $R = 16\text{nm}$  and Drude damping  $\gamma = \gamma_{\text{gold}}/4$  as a function of the number of benzene molecules.

boundary conditions at the material interfaces as appropriate. In this work we consider the situation where the emitter is placed in the inner region of the cavity, and it is therefore only necessary to consider the  $n = m = 3$  component of the DGF.

For a general emitter position inside the cavity, it is necessary to carefully converge the number of vector spherical harmonics used in the calculation of the DGF. However, if the emitter is placed exactly in the center of the cavity, the situation simplifies significantly. In this case, only the lowest order magnetic mode contributes and the reflection DGF can be written as [31],

$$\mathbf{G}_{33}^{\text{ref}}(\mathbf{r}, \mathbf{r}', \omega)|_{r, r' \rightarrow 0} = \frac{i\omega}{6\pi c} r_{n=1}^N(\omega) \mathbf{1}. \quad (20)$$

The imaginary part of the spatial trace of the vacuum DGF is given by  $\text{Im}\mathbf{G}^{\text{vac}}(\mathbf{r}, \mathbf{r}, \omega) = \frac{\omega}{6\pi c} \mathbf{1}$ . The imaginary part of the full DGF, evaluated in the center of the cavity  $\mathbf{0}$ , thus becomes,

$$\text{Im}\mathbf{G}(\mathbf{0}, \mathbf{0}, \omega) = \frac{\omega}{6\pi c} [1 + \text{Re}(r_{n=1}^N(\omega))] \mathbf{1}. \quad (21)$$

Notice that  $\mathbf{n}_i \cdot \text{Im}\mathbf{G}(\mathbf{0}, \mathbf{0}, \omega) \cdot \mathbf{n}_j \propto \delta_{ij}$  which means that the mode orthogonalization is trivial in this case, and the cavity field strengths can be derived directly,

$$\lambda_i(\omega) = e \left( \frac{\omega^2}{3\pi^2 \epsilon_0 c^3} [1 + \text{Re}(r_{n=1}^N(\omega))] \right)^{1/2} \hat{n}_i. \quad (22)$$

In practice, to use the QEDFT Casida formalism, it is necessary to employ a dense, discretized sampling of the continuous frequency expressions for the coupling strengths. This procedure is discussed in Supplementary note C. Furthermore, the details of the QEDFT calculations with these modes are given in Supplementary note D.

### Drude metal shell

We now consider the case where the inner and outer regions consist of vacuum. For the middle region we consider a simple, but realistic model of a metallic mirror, namely a Drude metal with dielectric function,

$$\epsilon_2(\omega) = 1 - \frac{\omega_p^2}{\omega^2 + i\gamma\omega}, \quad (23)$$

where  $\omega_p$  is the metal plasma frequency and  $\gamma$  is the Drude damping rate. As a concrete example of a metal, we use the Drude parameters for gold taken from Ref. [32]. Within the Drude mode, the plasma frequency of gold is around 8.5 eV [33]. This results in the dielectric function shown in Supplementary Figure 1b. Below the plasma frequency, the real part of the dielectric function will be negative and the material surface will consequently be highly reflective. Above the plasma frequency, the real part of the dielectric function becomes positive



and the material will lose its metallic characteristics resulting in a significant loss of surface reflectivity.

In Supplementary Figure 1c the mode structure of the cavity setup is shown for two different cavity radii,  $R = 140\text{nm}$  and  $R = 450\text{nm}$ . It is clearly observed that the number of modes, as well as their spectral position, is directly linked to the radius of the microcavity. Furthermore, we clearly observe that above the gold plasma frequency, the mirrors lose their reflectivity which results in the loss of the sharp mode structure which is replaced by a continuum. This highlights that the formalism we present is able to directly link the cavity field strengths to the real cavity setup made of real materials. Supplementary Figure 1d zooms in on the mode around 7.1 eV in the cavity with  $R = 140\text{nm}$  and shows the effect of changing the Drude damping parameter. We clearly observe that the width of the cavity mode increases with increasing damping in the metal which highlights the connection between the width of the cavity modes and the losses in the gold.

This example highlights how the use of the emitter centered representation of MQED allows us to directly and uniquely relate the light-matter coupling strength to a real electromagnetic environment and connect it to the QEDFT formalism. While this is a relatively simple example, the approach is general and works analogously for an arbitrary electromagnetic environment provided that the DGF can be determined.

### Adding an emitter to the cavity

We next add a benzene molecule to the cavity. Benzene is chosen mainly because of its prevalence as a test system in the existing TDDFT and QEDFT literature on strong coupling [11, 12, 15, 34], but we emphasize that the method can treat arbitrary finite electronic systems. We focus on finding a cavity configuration with a mode resonant with the  $\Pi \rightarrow \Pi^*$  transition of the benzene molecule. This transition is spectrally well isolated from other transitions. It thus represents an effective two level system for coupling strengths in the weak coupling and strong coupling regime, while care has to be taken in the ultrastrong coupling regime. The first step is to determine the spectral position of this transition. Using the Casida linear response QEDFT framework without photons, we find that the transition occurs at 6.808 eV (182 nm) in free space, consistent with previous TDDFT calculations for benzene [12, 15].

As shown in Fig. 1a, it is possible to find different radii of the gold microcavity for which there is a cavity mode resonant with the benzene  $\Pi \rightarrow \Pi^*$  electronic transition. As expected, the cavity field strength increases as the cavity is made smaller. All but the smallest cavity are optical cavities in the sense that the characteristic

dimension of the cavity, the radius, is larger than half the wavelength of the transition. For the smallest cavity of radius 16 nm, a significant increase in the coupling strength relative to the other sizes is observed. This happens exactly because this cavity is sub-wavelength sized and therefore significant near-field coupling to the surface plasmon mode of the gold starts to occur.

Fig. 1b shows the linear absorption spectra of the coupled emitter-cavity system calculated for the different cavity radii using the linear response QEDFT method. We emphasize that all linewidths in the figure are *true* linewidths in the sense that they are not related to any broadening parameters in the QEDFT calculation and only reflect the density of states in the optical environment. A radius-dependent Purcell enhancement with decreasing radius is clearly observed, reflecting the reduction in radiative lifetime resulting from the altered optical environment. However, it is not possible to achieve strong coupling with a single benzene molecule using the gold-shell cavity. We attribute this to the fact that as the coupling strength gets larger with decreasing radius, the optical losses also increase, resulting in a broader cavity resonance. We note in passing that the Purcell enhancement for the smallest  $R = 16\text{ nm}$  cavity is around 3500 which means that the local field enhancement at the center of the spherical microcavity is comparable to what is found in experiments with plasmonic microcavities [35].

The reason that it was impossible to reach strong coupling with benzene in the gold cavity was the losses of the cavity mode. In an attempt to reach the SC regime, we therefore next seek to reduce the losses in the cavity. As already discussed above, the width of the cavity resonance is reduced for smaller Drude damping parameters,  $\gamma$ . For this reason, Fig. 2a shows the absorption spectrum for the case with the true gold damping, as well as 25%, 10% and 5% of the damping respectively. We mention in passing that in practice one could imagine realizing these lower losses for example using metals specifically engineered to show weaker losses [36]. Furthermore, one could also imagine exploring different cavity setups potentially leveraging the lower losses in dielectric nano-optical setups [37]. Considering the wide range of available materials this design space becomes enormous [38, 39]. As shown in the inset of Fig. 2a, we find that reducing the losses results in a narrower cavity mode without a significant reduction in the overall cavity field strength. At around 25% of the true damping, we begin to observe clear indications of the two polariton peaks in the linear absorption spectrum. Further reducing the damping we see clear strong coupling with a Rabi splitting of around  $2g \sim 10\text{ eV}$ . This emphasizes the importance of the optical losses in reaching the strong coupling regime, and further highlights the significant strength of our method that we are able to study the

effect of different cavity parameters from first principles via our combination of QEDFT and MQED.

Another way to engineer the coupling strength is by changing the emitter. There are two ways to do this, either by changing the number of emitters or by changing the emitter itself. To investigate the first option, we take the cavity with 25% of the true gold losses, and compute the absorption spectrum for one, two and three benzene molecules, all of which we place in the center of the cavity. As shown in Fig. 2b, we see a clear evolution of the Rabi splitting with the number of benzene molecules indicating the onset of collective strong coupling [40–43]. To perform this analysis, one needs to solve a coupled many electron, many photon problem and it again highlights the strength of the method.

To investigate the latter option, we consider longer aromatic compounds with  $N$  aromatic rings; naphthalene ( $N = 2$ ), anthracene ( $N = 3$ ), tetracene ( $N = 4$ ) and pentacene ( $N = 5$ ). We first use the Casida method without photons (standard TDDFT) to characterize the spectral properties of the aromatic molecules. Fig. 3(a,b) shows respectively the spectrum and transition dipole moment of the  $\Pi \rightarrow \Pi^*$ -transition (HOMO-LUMO) as a function of the number of aromatic rings  $N$ . Note that in Fig. 3(a) the spectra are shown with the Octopus default artificial broadening of 0.1361 eV. This artificial broadening is necessary because unlike the combined MQED-QEDFT method, the standard photon-free TDDFT formulation fails to describe the linewidth of the transitions. We observe that with increasing number of aromatic rings  $N$ , the transition energy redshifts and the transition dipole moment increases linearly (Fig. 3(b)). The linearly increasing transition dipole moment would suggest that the light-matter coupling strength can be monotonically increased by simply using a larger aromatic molecule. However, because the transition energy also redshifts with increasing molecule length, the cavity has to be re-optimized to be resonant with the transition for each molecule, as shown in Fig. 3 (c). Specifically, focusing on modifications of the  $R = 16$  nm cavity, we find that this re-optimization of the cavity means that the cavity radius needs to be increased. This increase in radius leads to a reduced field concentration via an increased effective mode volume. This behavior highlights the important point that the light-matter coupling strength is a joint property of both the electronic system and the electromagnetic environment. A proper treatment of both is therefore essential for quantitative predictions.

We can characterize the intricate interplay between the electromagnetic environment and the electronic structure by looking at an effective coupling strength for the cavity modes which we define as [15],

$$g_{\text{eff}} \propto \sqrt{\omega_c} \lambda_c |\mathbf{d}|. \quad (24)$$

Here the total cavity field strength parameter is defined

as the coupling strength averaged across the cavity peak  $p$ ,  $\lambda_c = \sqrt{\int_p d\omega |\boldsymbol{\lambda}_d(\omega)|^2}$ , and  $\omega_c$  is the center frequency of the cavity mode. The  $d$  subscript indicates that we take the field strength parameter for dipole orientation  $\mathbf{d}/|\mathbf{d}|$ .  $g_{\text{eff}}$  would thus be the true light-matter coupling if the total spectral weight was concentrated in a single mode. As shown in Fig. 3d, we observe that the increase in transition dipole moment is counteracted by the reduced field concentration for the larger molecules, effectively resulting in a weaker light-matter coupling strength. This is in stark contrast to the intuitive argument based solely on the increased dipole moment of the longer molecules. It should be noted that  $g_{\text{eff}}$  is not a perfect measure of the light-matter coupling strength and it only gives a rough idea of the cavity re-optimization’s effect. This is because the widths of the modes are not taken into account which, as we have seen in Fig. 2a, is very important for the nature of the light-matter coupling.

We mention in passing that with the presented framework it would be possible to perform further engineering of the electromagnetic environment to increase the coupling for the larger aromatic compounds. The application of the framework to general electromagnetic environments is discussed further below.

## COMMENT ON FABRY PEROT CAVITIES

A common example of a cavity in the literature for both theory and experiments is the layered Fabry Perot cavity (FPC). As discussed in Supplementary note E, the FPC is a layered system and consequently its DGF is expanded in terms of in-plane plane waves, augmented by a function accounting for the reflection at the interfaces between the layers [20]. Because the FPC only constrains the electromagnetic modes in one direction, it retains significant dispersion of the modes in plane. Consequently, the concentration of electromagnetic density of states is significantly less efficient than in the case of e.g. the spherical microcavity. As discussed in Supplementary note E, this means that the resulting coupling strength is weaker and the FPC will therefore generally not be suited for single- or few emitter strong coupling [44]. For this reason, we do not perform explicit QEDFT calculations for this cavity setup. However, the FPC can still be suited for collective strong coupling [45] and coupling to extended systems [46] where the extended modes of the electromagnetic environment can be sampled more effectively.

## TOOL FOR CAVITY FIELD PARAMETERS IN SIMPLE CAVITIES

As a part of this work, we are making the code to generate the cavity field strengths available for everyone to

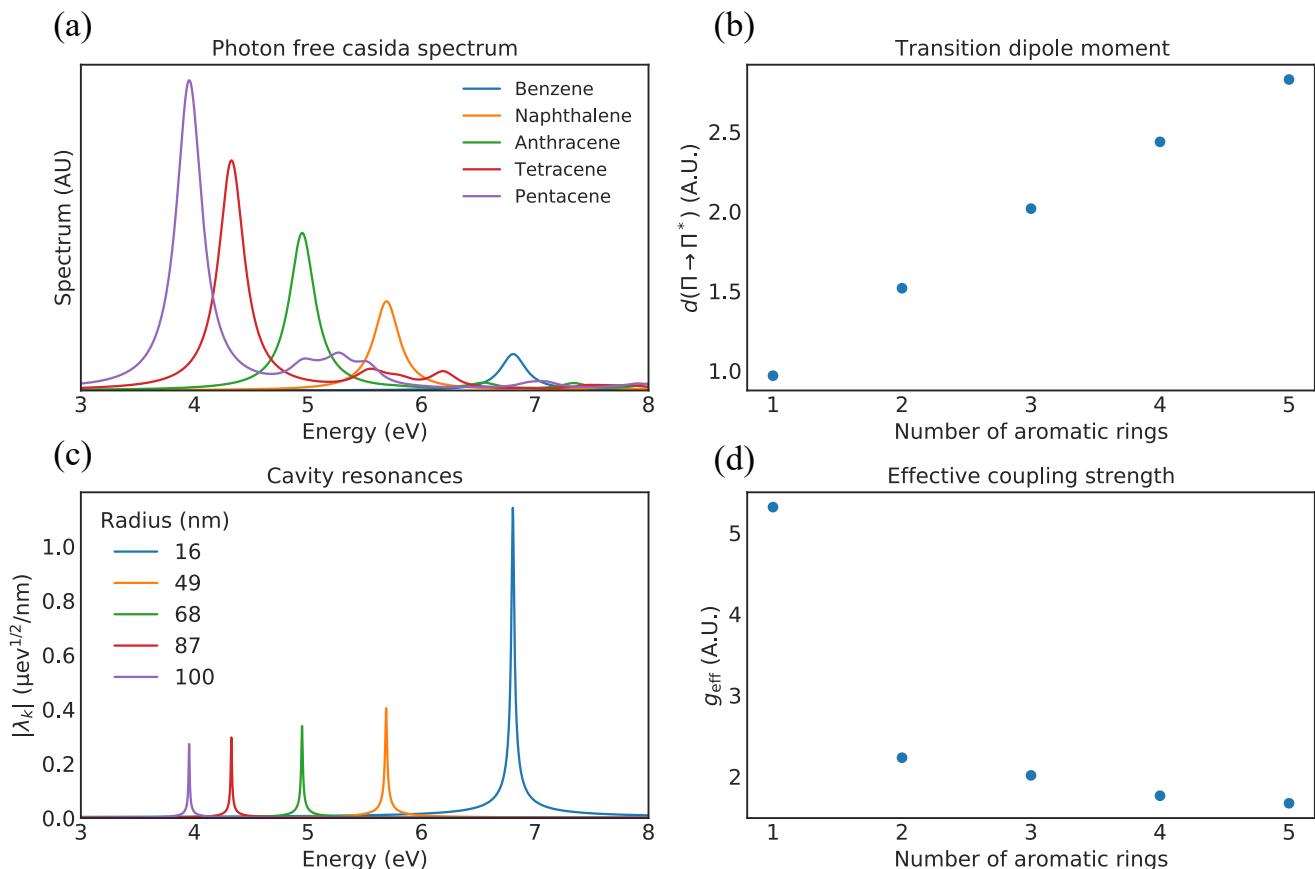


**FIG. 3.** (a) The Casida spectrum without photon modes for different aromatic compounds. The spectra here are shown with an artificial broadening of 0.1361 eV because the photon-free calculations fail to naturally describe the linewidth of the transitions. (b) Transition dipole moment of the  $\Pi \rightarrow \Pi^*$ -transition as a number of aromatic rings. (c) Mode structure of the smallest cavities which host resonances aligned with the  $\Pi \rightarrow \Pi^*$ -transition of the different molecules. The mode structure is shown with a sampling density of 10 points/meV. (d) Effective light-matter coupling strength as a function of the number of benzene rings in the aromatic molecule.

use as part of the new [PhotonPilot](#) tool. This tool currently allows the user to calculate cavity field strengths for the spherical and layered cavity setups, and we plan to expand its capabilities in the future.

### GENERAL ELECTROMAGNETIC ENVIRONMENTS

We emphasize that the method we have presented here is general and applicable to any electromagnetic environment as long as the DGF can be determined. However, in general electromagnetic environments with lower symmetry it is not possible to write down an analytical expression for the DGF. In such cases, the DGF must be constructed numerically from e.g. a mode expansion based on finite element simulations [20, 25]. We note in passing that in the general setting the Helmholtz equation is not a Hermitian operator. Special care is therefore needed when constructing the spectral representation of the DGF from the modes. One solution is to use the

biorthonormal construction discussed in Ref. [47]. We envision that the method presented in this paper will eventually be integrated with the existing Maxwell solver in the Octopus code[48, 49]. Such an integration would allow for the treatment of general electromagnetic environments completely within Octopus.

### CONCLUSION

In this paper, we have presented a methodology combining macroscopic quantum electrodynamics with quantum-electrodynamical density-functional theory which provides a fully ab-initio description of coupled quantum light-matter systems. To exemplify this approach, we have considered a benzene molecule strongly coupled to a metallic spherical cavity and investigated the impact of the both cavity radius and cavity loss on the nature of the light-matter coupling. We have further investigated the effect of adding more molecules and exchanging benzene with larger aromatic molecules. Together,



these results highlight the intricate interplay between the electronic structure of the emitter and the environment in determining the nature of the light-matter coupling. Our work therefore illustrates the importance of having a proper description of both the electronic system and the electromagnetic environment for a proper description of quantum light-matter interactions. This work sets out the direction for more quantitative calculations in the future and also opens the possibility for the proper treatment of real experimental setups. We emphasize that the connection between the optical environment and the DGF is not limited to setups similar to cavities, but instead provides a general way to determine the electromagnetic spectral density of an arbitrary environment. In addition to the QED setup, our method therefore also provides a way to perform time-dependent density-functional theory in a lossy optical environment and removes the need for artificial spectral broadening.

Finally, we have provided an easy to use tool that everyone can use to generate cavity parameters for simple cavities such as the spherical microcavity or a layered cavity.

#### ACKNOWLEDGEMENTS:

All calculations were performed using the computational facilities of the Flatiron Institute. The Flatiron Institute is a division of the Simons Foundation. We acknowledge support from the Max Planck-New York City Center for Non-Equilibrium Quantum Phenomena.

K.S.T. acknowledges funding from the European Research Council (ERC) under the European Union's Horizon 2020 research and innovation program grant no. 773122 (LIMA). K.S.T. is a Villum Investigator supported by VILLUM FONDEN (grant no. 37789)

---

\* mark-kamper.svendsen@mpsd.mpg.de

- [1] F. Benz, M. K. Schmidt, A. Dreismann, R. Chikkaraddy, Y. Zhang, A. Demetriadou, C. Carnegie, H. Ohadi, B. de Nijs, R. Esteban, J. Aizpurua, and J. J. Baumberg, Single-molecule optomechanics in picocavities, *Science* **354**, 726 (2016), <https://www.science.org/doi/pdf/10.1126/science.aah5243>.
- [2] A. Pscherer, M. Meierhofer, D. Wang, H. Kelkar, D. Martín-Cano, T. Utikal, S. Götzinger, and V. Sandoghdar, Single-molecule vacuum rabi splitting: Four-wave mixing and optical switching at the single-photon level, *Phys. Rev. Lett.* **127**, 133603 (2021).
- [3] T. T. H. Do, M. Nonahal, C. Li, V. Valuckas, A. I. Kuznetsov, H. S. Nguyen, I. Aharonovich, and S. T. Ha, Room-temperature strong coupling in a single photon emitter-dielectric metasurface system (2022).
- [4] B. Munkhbat, A. Canales, B. Küçüköz, D. G. Baranov, and T. O. Shegai, Tunable self-assembled casimir microcavities and polaritons, *Nature* **597**, 214 (2021).
- [5] N. S. Mueller, Y. Okamura, B. G. M. Vieira, S. Juerghen, H. Lange, E. B. Barros, F. Schulz, and S. Reich, Deep strong light-matter coupling in plasmonic nanoparticle crystals, *Nature* **583**, 780 (2020).
- [6] D. N. Basov, A. Asenjo-Garcia, P. J. Schuck, X. Zhu, and A. Rubio, Polariton panorama, *Nanophotonics* **10**, 549 (2020).
- [7] B. S. Simpkins, A. D. Dunkelberger, and I. Vurgaftman, Control, modulation, and analytical descriptions of vibrational strong coupling, *Chemical Reviews* (2023).
- [8] M. Ruggenthaler, J. Flick, C. Pellegrini, H. Appel, I. V. Tokatly, and A. Rubio, Quantum-electrodynamical density-functional theory: Bridging quantum optics and electronic-structure theory, *Physical Review A* **90**, 012508 (2014).
- [9] W. Kohn, Nobel lecture: Electronic structure of matter-wave functions and density functionals, *Rev. Mod. Phys.* **71**, 1253 (1999).
- [10] C. Pellegrini, J. Flick, I. V. Tokatly, H. Appel, and A. Rubio, Optimized effective potential for quantum electrodynamical time-dependent density functional theory, *Physical Review Letters* **115**, 093001 (2015).
- [11] J. Flick, C. Schäfer, M. Ruggenthaler, H. Appel, and A. Rubio, Ab initio optimized effective potentials for real molecules in optical cavities: Photon contributions to the molecular ground state, *ACS photonics* **5**, 992 (2018).
- [12] J. Flick, D. M. Welakuh, M. Ruggenthaler, H. Appel, and A. Rubio, Light-matter response in nonrelativistic quantum electrodynamics, *ACS photonics* **6**, 2757 (2019).
- [13] J. Yang, Q. Ou, Z. Pei, H. Wang, B. Weng, Z. Shuai, K. Mullen, and Y. Shao, Quantum-electrodynamical time-dependent density functional theory within gaussian atomic basis, *The Journal of Chemical Physics* **155**, 064107 (2021).
- [14] C. Schäfer, J. Flick, E. Ronca, P. Narang, and A. Rubio, Shining light on the microscopic resonant mechanism responsible for cavity-mediated chemical reactivity, *Nature Communications* **13**, 10.1038/s41467-022-35363-6 (2022).
- [15] D. S. Wang, T. Neuman, J. Flick, and P. Narang, Light-matter interaction of a molecule in a dissipative cavity from first principles, *The Journal of Chemical Physics* **154**, 104109 (2021).
- [16] A. Kudlis, I. Iorsh, and I. Tokatly, Dissipation and spontaneous emission in quantum electrodynamical density functional theory based on optimized effective potential: A proof of concept study, arXiv preprint arXiv:2111.04523 (2021).
- [17] S. Scheel and S. Y. Buhmann, Macroscopic qed-concepts and applications, *acta physica slovacica*, 675 (2008).
- [18] M. K. Svendsen, Y. Kurman, P. Schmidt, F. Koppens, I. Kaminer, and K. S. Thygesen, Combining density functional theory with macroscopic qed for quantum light-matter interactions in 2d materials, *Nature communications* **12**, 1 (2021).
- [19] J. Feist, A. I. Fernández-Domínguez, and F. J. García-Vidal, Macroscopic qed for quantum nanophotonics: emitter-centered modes as a minimal basis for multiemitter problems, *Nanophotonics* **10**, 477 (2021).
- [20] W. C. Chew, *Waves and fields in inhomogeneous media*, Vol. 16 (John Wiley & Sons, 1999).
- [21] R. G. Woolley, Gauge invariant wave mechanics and the

- power-zienau-woolley transformation, *J. Phys. A: Math. Gen* **13**, 2795 (1980).
- [22] M. Babiker and R. Loudon, Derivation of the power-zienau-woolley hamiltonian in quantum electrodynamics by gauge transformation, *Proc. R. Soc. London, A* **385**, 439 (1983).
- [23] S. Y. Buhmann and D. G. Welsch, Casimir-Polder forces on excited atoms in the strong atom-field coupling regime, *Physical Review A - Atomic, Molecular, and Optical Physics* **77**, 10.1103/PhysRevA.77.012110 (2008).
- [24] T. Hümmer, F. J. García-Vidal, L. Martín-Moreno, and D. Zueco, Weak and strong coupling regimes in plasmonic QED, *Physical Review B - Condensed Matter and Materials Physics* **87**, 10.1103/PhysRevB.87.115419 (2013), [arXiv:1209.1724](https://arxiv.org/abs/1209.1724).
- [25] L. Novotny and B. Hecht, *Principles of nano-optics* (Cambridge university press, 2012).
- [26] I. V. Tokatly, Time-dependent density functional theory for many-electron systems interacting with cavity photons, *Physical review letters* **110**, 233001 (2013).
- [27] D. M. Welakuh, J. Flick, M. Ruggenthaler, H. Appel, and A. Rubio, Frequency-dependent sternheimer linear-response formalism for strongly coupled light-matter systems, *Journal of Chemical Theory and Computation* **18**, 4354 (2022), pMID: 35675628, <https://doi.org/10.1021/acs.jctc.2c00076>.
- [28] M. E. Casida, Time-dependent density functional response theory for molecules, in *Recent Advances In Density Functional Methods: (Part I)* (World Scientific, 1995) pp. 155–192.
- [29] C. Schäfer, F. Buchholz, M. Penz, M. Ruggenthaler, and A. Rubio, Making ab initio qed functional (s): Non-perturbative and photon-free effective frameworks for strong light-matter coupling, *Proceedings of the National Academy of Sciences* **118**, e2110464118 (2021).
- [30] J. Flick, Simple exchange-correlation energy functionals for strongly coupled light-matter systems based on the fluctuation-dissipation theorem, *Phys. Rev. Lett.* **129**, 143201 (2022).
- [31] H. T. Dung, L. Knöll, and D.-G. Welsch, Spontaneous decay in the presence of dispersing and absorbing bodies: General theory and application to a spherical cavity, *Physical Review A* **62**, 053804 (2000).
- [32] M. G. Blaber, M. D. Arnold, and M. J. Ford, Search for the ideal plasmonic nanoshell: the effects of surface scattering and alternatives to gold and silver, *The Journal of Physical Chemistry C* **113**, 3041 (2009).
- [33] It should be noted that the Drude model is not a good model for the dielectric properties of gold due to the neglect of d-band absorption. Additionally, it should be mentioned that the Drude model will fail to account for size dependent resonance shifts and broadening resulting from the nonlocal response and surface enhanced Landau dampening in small metallic structures [50, 51].
- [34] T. P. Rossi, T. Shegai, P. Erhart, and T. J. Antosiewicz, Strong plasmon-molecule coupling at the nanoscale revealed by first-principles modeling, *Nature communications* **10**, 3336 (2019).
- [35] G. M. Akselrod, C. Argyropoulos, T. B. Hoang, C. Ciraci, C. Fang, J. Huang, D. R. Smith, and M. H. Mikkelsen, Probing the mechanisms of large purcell enhancement in plasmonic nanoantennas, *Nature Photonics* **8**, 835 (2014).
- [36] M. N. Gjerding, M. Pandey, and K. S. Thygesen, Band structure engineered layered metals for low-loss plasmonics, *Nature communications* **8**, 15133 (2017).
- [37] A. I. Kuznetsov, A. E. Miroschnichenko, M. L. Brongersma, Y. S. Kivshar, and B. Luk'yanchuk, Optically resonant dielectric nanostructures, *Science* **354**, aag2472 (2016).
- [38] D. G. Baranov, D. A. Zuev, S. I. Lepeshov, O. V. Kotov, A. E. Krasnok, A. B. Evlyukhin, and B. N. Chichkov, All-dielectric nanophotonics: the quest for better materials and fabrication techniques, *Optica* **4**, 814 (2017).
- [39] M. K. Svendsen, H. Sugimoto, A. Assadillayev, D. Shima, M. Fujii, K. S. Thygesen, and S. Raza, Computational discovery and experimental demonstration of boron phosphide ultraviolet nanoresonators, *Advanced Optical Materials* **10**, 2200422 (2022).
- [40] T. W. Ebbesen, Hybrid light-matter states in a molecular and material science perspective, *Accounts of chemical research* **49**, 2403 (2016).
- [41] C. Genet, J. Faist, and T. W. Ebbesen, Inducing new material properties with hybrid light-matter states, *Physics Today* **74**, 42 (2021).
- [42] D. Sidler, M. Ruggenthaler, C. Schäfer, E. Ronca, and A. Rubio, A perspective on ab initio modeling of polaritonic chemistry: The role of non-equilibrium effects and quantum collectivity, *The Journal of Chemical Physics* **156**, 230901 (2022).
- [43] M. Ruggenthaler, D. Sidler, and A. Rubio, Understanding polaritonic chemistry from ab initio quantum electrodynamics, *arXiv preprint arXiv:2211.04241* (2022).
- [44] S. Dutra and P. Knight, Spontaneous emission in a planar fabry-pérot microcavity, *Physical Review A* **53**, 3587 (1996).
- [45] A. Thomas, L. Lethuillier-Karl, K. Nagarajan, R. M. A. Vergauwe, T. C. J. George, A. Shalabney, E. Devaux, C. Genet, J. Moran, and T. W. Ebbesen, Tilting a ground-state reactivity landscape by vibrational strong coupling, *Science* **364**, 615 (2019).
- [46] J. Gu, V. Walther, L. Waldecker, D. Rhodes, A. Raja, J. C. Hone, T. F. Heinz, S. Kéna-Cohen, T. Pohl, and V. M. Menon, Enhanced nonlinear interaction of polaritons via excitonic rydberg states in monolayer WSe<sub>2</sub>, *Nature Communications* **12**, 10.1038/s41467-021-22537-x (2021).
- [47] Y. Chen, T. R. Nielsen, N. Gregersen, P. Lodahl, and J. Mørk, Finite-element modeling of spontaneous emission of a quantum emitter at nanoscale proximity to plasmonic waveguides, *Physical Review B* **81**, 125431 (2010).
- [48] N. Tancogne-Dejean, M. J. Oliveira, X. Andrade, H. Appel, C. H. Borca, G. Le Breton, F. Buchholz, A. Castro, S. Corni, A. A. Correa, *et al.*, Octopus, a computational framework for exploring light-driven phenomena and quantum dynamics in extended and finite systems, *The Journal of chemical physics* **152**, 124119 (2020).
- [49] R. Jestädt, M. Ruggenthaler, M. J. Oliveira, A. Rubio, and H. Appel, Light-matter interactions within the ehrenfest-maxwell-pauli-kohn framework: fundamentals, implementation, and nano-optical applications, *Advances in Physics* **68**, 225 (2019).
- [50] N. A. Mortensen, S. Raza, M. Wubs, T. Søndergaard, and S. I. Bozhevolnyi, A generalized non-local optical response theory for plasmonic nanostructures, *Nature communications* **5**, 3809 (2014).
- [51] M. Svendsen, C. Wolff, A.-P. Jauho, N. A. Mortensen, and C. Tserkezis, Role of diffusive surface scattering in

nonlocal plasmonics, *Journal of Physics: Condensed Matter* **32**, 395702 (2020).

- [52] S. Mukamel, *Principles of nonlinear optical spectroscopy*, 6 (Oxford University Press on Demand, 1999).  
 [53] J. Flick, N. Rivera, and P. Narang, Strong light-matter coupling in quantum chemistry and quantum photonics, *Nanophotonics* **7**, 1479 (2018).  
 [54] I. Medina, F. J. García-Vidal, A. I. Fernández-

Domínguez, and J. Feist, Few-mode field quantization of arbitrary electromagnetic spectral densities, *Physical Review Letters* **126**, 093601 (2021).

- [55] M. Sánchez-Barquilla, F. J. García-Vidal, A. I. Fernández-Domínguez, and J. Feist, Few-mode field quantization for multiple emitters, *Nanophotonics* **11**, 4363 (2022).

## SUPPLEMENTARY INFORMATION

### Supplementary note A: Length-gauge Pauli Fierz Hamiltonian in terms of the emitter centered modes

Our starting point is the PZW gauge Hamiltonian describing an electronic system coupled to the MQED field within the dipole approximation [17]. Neglecting magnetic interactions, the Hamiltonian reads,

$$\begin{aligned} \mathcal{H} = & \sum_{\alpha} \frac{\hat{\mathbf{p}}_{\alpha}^2}{2m_{\alpha}} + \frac{1}{2\epsilon_0} \int d\mathbf{r} \hat{\mathbf{P}}(\mathbf{r})^2 \\ & + \sum_{\lambda} \int_0^{\infty} d\omega \hbar\omega \int d\mathbf{r} \hat{\mathbf{f}}_{\lambda}^{\dagger}(\mathbf{r}, \omega) \cdot \hat{\mathbf{f}}_{\lambda}(\mathbf{r}, \omega) - \hat{\mathbf{d}} \cdot \hat{\mathbf{E}}(\mathbf{r}_0). \end{aligned} \quad (\text{A1})$$

To connect this to the Hamiltonian used in the Octopus code QEDFT implementation[12],

$$\hat{H}_0 = \hat{H}_e + \frac{1}{2} \sum_{\alpha=1}^N \left( \hat{p}_{\alpha}^2 + \omega_{\alpha}^2 \left[ \hat{q}_{\alpha} + \frac{\boldsymbol{\lambda}_{\alpha}}{\omega_{\alpha}} \cdot \hat{\mathbf{R}} \right]^2 \right), \quad (\text{A2})$$

we follow Ref. [15] in defining the cavity field strength,  $\boldsymbol{\lambda}_i(\omega) = -\left(\frac{2}{\hbar\omega}\right)^{1/2} e\mathbf{E}_i(\mathbf{r}_0, \omega)$ , and rewrite the emitter-centered representation of the MQED field in Eq. 6 from the manuscript as,

$$\hat{\mathbf{E}}(\mathbf{r}_0) = - \sum_i \int_0^{\infty} d\omega \left( \frac{\hbar\omega}{2e^2} \right)^{1/2} \boldsymbol{\lambda}_i(\omega) \hat{C}_i(\omega) + \text{h.c.} \quad (\text{A3})$$

Next we want to change from the ladder operators to the canonical operators,  $\hat{q}_i(\omega) = \left(\frac{\hbar}{2\omega}\right)^{1/2} (\hat{C}_i(\omega) + \hat{C}_i^{\dagger}(\omega))$  and  $\hat{p}_i(\omega) = \left(\frac{\hbar\omega}{2}\right)^{1/2} (\hat{C}_i(\omega) - \hat{C}_i^{\dagger}(\omega))$ , again to be consistent with the Octopus implementation of QEDFT. This is possible as long as the orthogonalization scheme used in the construction of  $\hat{C}_i(\omega)$  results in real valued  $\mathbf{V}(\omega)$  matrices. With this change, the electric field operator becomes,

$$\hat{\mathbf{E}}(\mathbf{r}_0) = - \sum_i \int_0^{\infty} d\omega \frac{\omega}{e} \boldsymbol{\lambda}_i(\omega) \hat{q}_i(\omega). \quad (\text{A4})$$

The idea is then to use Eq. A4 to put Eq. A1 in a form similar to the Hamiltonian in Eq. A2. The intuitive generalization of the Hamiltonian to the continuous case suggests that,

$$\begin{aligned} \mathcal{H} = & \mathcal{H}_{\text{Mat}}^{\text{C}} + \\ & \frac{1}{2} \sum_i \int_0^{\infty} d\omega \left\{ \hat{p}_i(\omega)^2 + \omega^2 \left[ \hat{q}_i(\omega) + \frac{\boldsymbol{\lambda}_i(\omega)}{\omega} \cdot \hat{\mathbf{R}} \right]^2 \right\}. \end{aligned} \quad (\text{A5})$$

Here  $\hat{\mathbf{R}} = \sum_i \hat{\mathbf{r}}_i$  is the center of mass position of the charges making up the emitter which is related to the dipole moment as  $\hat{\mathbf{d}} = -e\hat{\mathbf{R}}$ . The question is then under what conditions this holds. Inserting the field expansion into the emitter-field coupling term in the Hamiltonian results in,

$$\hat{H}_{\text{int}} = -\hat{\mathbf{d}} \cdot \hat{\mathbf{E}}(\mathbf{r}_0) = \sum_i \int_0^{\infty} d\omega \omega \left[ \boldsymbol{\lambda}_i(\omega) \cdot \hat{\mathbf{R}} \right] \hat{q}_i(\omega). \quad (\text{A6})$$

which is the straightforward generalization of the lossless case.

The other term in which the field parameters appear is the dipole self energy term. This term should generally be derived in terms of the transverse projection of the full polarization term[52],

$$\hat{\mathbf{P}}_{\perp}(\mathbf{r}) = \frac{2}{3}\hat{\mathbf{P}}(\mathbf{r}) + \int d\mathbf{r}' \hat{\mathbf{T}}_{\perp}(\mathbf{r}, \mathbf{r}') \cdot \hat{\mathbf{P}}(\mathbf{r}'). \quad (\text{A7})$$

However, the direct application of this projection is computationally cumbersome. In the lossless case, the Helmholtz equation is Hermitian and its transverse solutions form a orthogonal and complete basis for the transverse space. Consequently, the transverse polarization can be expanded in terms of these modes and the projection can be simplified significantly. This procedure leads to the standard form of the dipole self-energy term,

$$\frac{1}{2\epsilon_0} \int d\mathbf{r} [\hat{\mathbf{P}}_{\perp}(\mathbf{r})]^2 = \frac{1}{2} \sum_{\alpha} [\boldsymbol{\lambda}_{\alpha} \cdot \hat{\mathbf{R}}]^2. \quad (\text{A8})$$

The fact that the transverse modes can be used to span the transverse projector indicates that any truncation of the photon Hilbert space needs to be performed carefully as it indirectly results in a truncation of the transverse basis and therefore also the transverse polarization. The two should therefore generally always be truncated consistently[53].

The expansion of the transverse polarization field in the presence of losses is more complicated. If the cavity losses are not true absorptive losses, but simply a result of e.g. finite reflectivity of the cavity mirrors, the modes will globally obey,

$$\int d\mathbf{r} \mathbf{E}_i(\mathbf{r}, \omega_1) \cdot \mathbf{E}_j(\mathbf{r}, \omega_2) = \delta_{ij} \delta(\omega_1 - \omega_2), \quad (\text{A9})$$

and thus remain orthogonal and complete. In this case the transverse polarization can be straightforwardly generalized,

$$\frac{1}{2\epsilon_0} \int d\mathbf{r} [\hat{\mathbf{P}}_{\perp}(\mathbf{r})]^2 = \frac{1}{2} \sum_i \int_0^{\infty} d\omega [\boldsymbol{\lambda}_i(\omega) \cdot \hat{\mathbf{R}}]^2. \quad (\text{A10})$$

In the presence of true absorption losses it is not possible to define the transverse projector in terms of the field modes because these no longer form a complete, orthonormal set. We speculate that the transverse projection should instead be defined in terms of a biorthonormal construction as discussed in Ref. [47]. From the point of the emitter it should not be possible to distinguish these two cases because it only samples the field at its position. We thus speculate that, at least for a single emitter position, the true form of the dipole self energy term in the presence of losses will functionally be no different than Eq. A10. For multiple emitter positions it is unlikely that the dipole self-energy term can be expanded directly in terms of the mode functions, and we will explore this further in future research.

### Supplementary note B: Dyadic Green's Function of the spherical microcavity

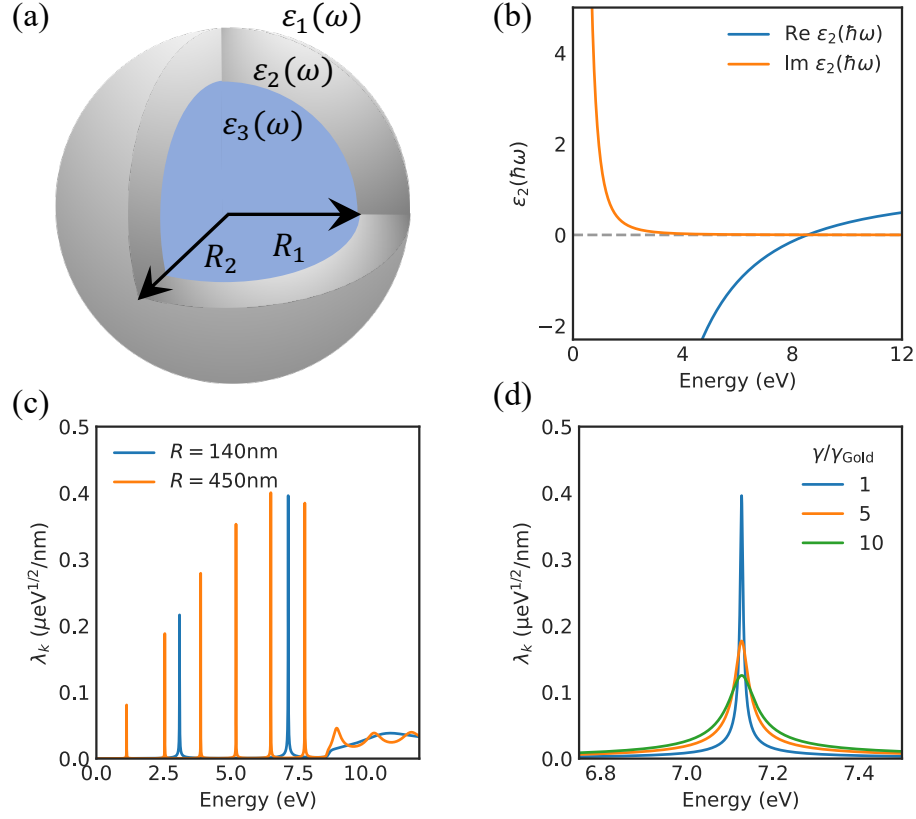
We consider the spherically layered microcavity from Ref. [31]. To use the emitter centered framework, the DGF must be derived. In general, the source and field points ( $\mathbf{r}$  and  $\mathbf{r}'$  respectively) can be in either the same layer or different layers. Consequently, the DGF for the reflected field is a 9 component object, where each component is a 3D dyad. Labelling the possible combinations of source and field points by two extra indices  $m, n = 1, 2, 3$ , the full DGF of the system can be written as,

$$\mathbf{G}_{mn}(\mathbf{r}, \mathbf{r}', \omega) = \mathbf{G}^{\text{vac}}(\mathbf{r}, \mathbf{r}', \omega) \delta_{nm} + \mathbf{G}_{mn}^{\text{ref}}(\mathbf{r}, \mathbf{r}', \omega). \quad (\text{B1})$$

Due to the spherical symmetry of the problem, the DGF of the system is most efficiently expanded onto vector spherical harmonics. The 9 different components of the reflection contribution can be worked out by invoking the electromagnetic boundary conditions at the material interfaces. In this work we consider the situation where the emitter is placed in the inner region of the cavity, and it is therefore only necessary to consider the  $n = m = 3$  component of the DGF.

For a general emitter position inside the cavity, it is necessary to carefully converge the number of vector spherical harmonics used in the calculation of the DGF. However, if the emitter is placed exactly in the center of the cavity things simplify significantly. In this case, only the lowest order transverse magnetic mode contributes and the reflection DGF can be written as[31],

$$\mathbf{G}_{33}^{\text{ref}}(\mathbf{r}, \mathbf{r}', \omega)|_{r, r' \rightarrow 0} = \frac{i\omega}{6\pi c} r_{n=1}^N(\omega) \mathbb{1}. \quad (\text{B2})$$



**Supplementary Figure 1. Spherical microcavity setup:** (a) Illustration of the three layer spherical microcavity setup. (b) The Drude model dielectric function of gold. (c) The modes of the spherical microcavity plotted for two different radii,  $R = 140\text{nm}$  in blue and  $R = 450\text{nm}$  in orange. The mode structure is shown with a sampling density of 10 points/meV. (d) The impact from the Drude damping parameter on the cavity resonances, illustrated by focusing on the mode around 7.1 eV in the cavity with  $R = 140\text{nm}$ .

where  $r_{n=1}^N(\omega)\mathbf{1}$  is the reflection coefficient for the lowest order transverse magnetic mode. If we assume that region 2 is very thick we can write[31],

$$r_{n=1}^N(\omega) = \frac{\left[ i + \rho(n(\omega) + 1) - i\rho^2 n(\omega) - \frac{\rho^3 n(\omega)^2}{n(\omega)+1} \right] e^{i\rho}}{\sin\rho - \rho(\cos\rho + in(\omega)\sin\rho) + i\rho^2 n(\omega)\cos\rho - \rho^3(\cos\rho - in(\omega)\sin\rho) \frac{n(\omega)^2}{n(\omega)^2-1}}, \quad (\text{B3})$$

where  $\rho = R\omega/c$  is the standard size parameter from Mie theory[25].

The contribution from the vacuum DGF is  $\text{Im}\mathbf{G}^{\text{vac}}(\mathbf{r}, \mathbf{r}, \omega) = \frac{\omega}{6\pi c}\mathbf{1}$ . The imaginary part of the full DGF, evaluated in the center of the cavity, thus becomes,

$$\text{Im}\mathbf{G}(\mathbf{0}, \mathbf{0}, \omega) = \frac{\omega}{6\pi c} \left[ 1 + \text{Re}r_{n=1}^N(\omega) \right] \mathbf{1}. \quad (\text{B4})$$

Denoting the unit vector in the  $i$ 'th direction  $\mathbf{n}_i$  it can be noticed that,  $\mathbf{n}_i \cdot \text{Im}\mathbf{G}(\mathbf{0}, \mathbf{0}, \omega) \cdot \mathbf{n}_j \propto \delta_{ij}$  which means that the mode orthogonalization needed in the emitter centered formulation is trivial in this case. The cavity field parameters can therefore be derived directly,

$$\boldsymbol{\lambda}_i(\omega) = -e \left( \frac{\omega^2}{3\pi^2 \epsilon_0 c^3} \left[ 1 + \text{Re}r_{n=1}^N(\omega) \right] \right)^{1/2} \mathbf{n}_i. \quad (\text{B5})$$

Notice that the spherical symmetry of the cavity means that at each frequency there are three orthogonal modes with identical field strengths, differing only by their spatial orientation  $i$ . Any dipole orientation therefore couples identically to the cavity modes if the emitter is placed in the center of the cavity.



### Supplementary note C: Discretization of the cavity coupling parameters

In practice, we need to discretize the continuous expressions for the cavity field strengths,  $\lambda(\omega)$ . The idea is then to sample densely enough to mimic a true continuum of modes. This means that the sampling density should be converged in the simulations. If we assume that we have uniformly spaced modes we can perform the simple discretization,

$$\int_0^\infty d\omega \rightarrow \sum_k \Delta\omega. \quad (\text{C1})$$

In the continuous formulation, the operators  $\hat{C}_i(\omega)$  have units of  $\text{s}^{1/2}$  and the field,  $\mathbf{E}(\mathbf{r}, \omega)$  has units of  $\text{Vs}^{1/2}/\text{m}$ . It therefore makes sense to define the a new discretized field and creating/annihilation operators as,

$$\mathbf{E}_k(\omega_k) \equiv \sqrt{\Delta\omega} \mathbf{E}_i(\mathbf{0}, \omega_k), \quad (\text{C2})$$

$$\hat{a}_k^{(\dagger)} \equiv \sqrt{\Delta\omega} \hat{C}_i^{(\dagger)}(\omega). \quad (\text{C3})$$

This also means that we should write,

$$\lambda_k = -e \left( \frac{\Delta\omega\omega_k^2}{3\pi^2\epsilon_0 c^3} [1 + \text{Re } r_{m=1}^N(\omega_k)] \right)^{1/2} \hat{n}_i. \quad (\text{C4})$$

### Supplementary note D: Computational details for the QEDFT calculations

We use the publicly available real space psuedo-potential DFT code OCTOPUS[48]. Molecular geometries are optimized with the LDA exchange-correlation functional, on a real space grid consisting of spheres of radius  $6\text{\AA}$  around each atom with a grid spacing of  $0.16\text{\AA}$ .

We also calculate the ground state using the LDA exchange-correlation functional on a real space grid consisting of spheres of radius  $6\text{\AA}$  around each atom with a grid spacing of  $0.08\text{\AA}$ . We perform a fixed-density calculation on top of the ground state calculation to determine the excited states needed for the Casida calculation for which we use 500 excited states. These parameters ensure that the relevant transitions are converged to within  $1\text{ meV/atom}$ .

We employ uniform sampling of the electromagnetic environment and converge each calculation separately. In general, we find good convergence when sampling each cavity peak with around 1000 photon modes. While the current work employs uniform sampling, we note that more efficient methods for sampling the electromagnetic environment has recently been introduced in the context of master equation approaches [54, 55]. In the future, it would therefore be interesting to investigate whether similar approaches can be applied to photon mode sampling within the framework presented in the current work.

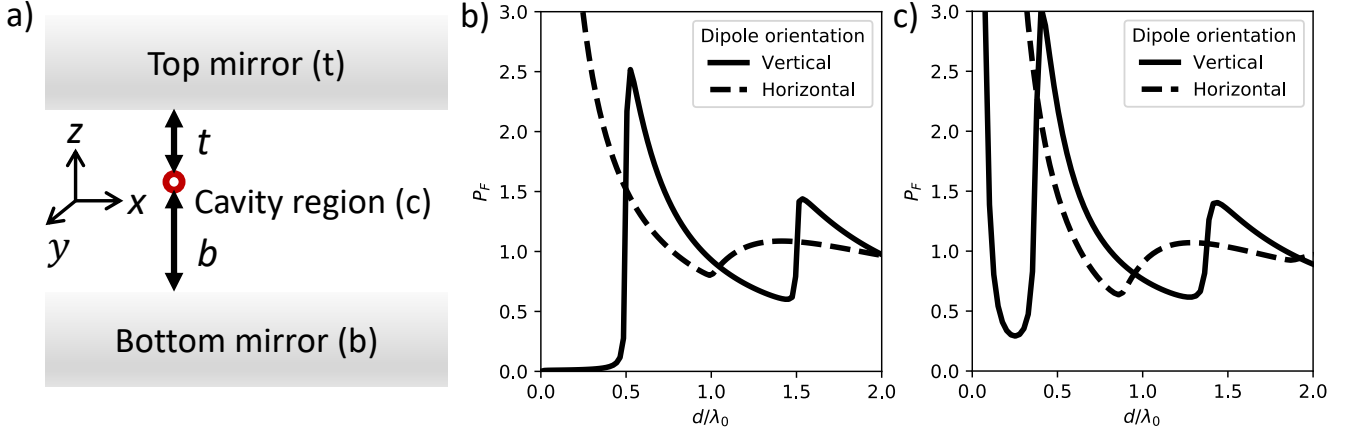
### Supplementary note E: The Fabry Perot cavity

In this supplementary note we briefly discuss the widely used Fabry Perot cavity (FPC). As shown in Supplementary Figure 2, the stereotypical FPC is a stratified system. Consequently, its DGF can be conveniently represented in the angular spectrum representation. Considering just the cavity region, the DGF can be written as[20],

$$\mathbf{G}(\mathbf{r}, \mathbf{r}', \omega) = \frac{i}{8\pi^2} \int \frac{d\mathbf{q}}{k_z q^2} [\mathbf{M}(\mathbf{q}, \mathbf{r}, \mathbf{r}') + \mathbf{N}(\mathbf{q}, \mathbf{r}, \mathbf{r}')]. \quad (\text{E1})$$

Here  $\mathbf{q}$  is the in-plane wave vector,  $k_z = \sqrt{k^2 - q^2}$  is the out of plane wave vector where  $k$  is the wave number in the medium and  $q = |\mathbf{q}|$ .  $\mathbf{M}$  and  $\mathbf{N}$  are the tensorial contributions from the TE and TM polarized modes respectively. These tensors can be found by solving the scattering from a point source in a layered medium as discussed in detail in e.g. Refs. [20, 25]. Importantly, if we consider a single emitter position in the FPC, we only need information about the  $\mathbf{r} = \mathbf{r}'$  part of the DGF to describe the coupling to the electromagnetic environment. Conveniently, at  $\mathbf{r} = \mathbf{r}'$  both  $\mathbf{M}$  and  $\mathbf{N}$  are diagonal matrices when expressed in cylindrical coordinates with the  $z$ -axis perpendicular to the mirrors,

$$k_x = q \cos \phi, \quad k_y = q \sin \phi, \quad k_z = k_z. \quad (\text{E2})$$



**Supplementary Figure 2. The Fabry Perot cavity:** a) Paradigmatic sketch of a Fabry Perot Cavity. b) Purcell enhancement as a function of  $d/\lambda_0$  for both vertical and horizontal dipole orientations when considering idealized mirrors with a frequency independent reflectivity  $R = 0.95$ . c) Purcell enhancement as a function of  $d/\lambda_0$  for both vertical and horizontal dipole orientations when considering metal mirrors with dielectric functions described by the Drude model in Eq. 23.

This is also the natural choice because the in-plane wave number  $q = \sqrt{k_x^2 + k_y^2}$  is the natural variable in the stratified FPC. The integration over  $\phi$  can be performed analytically which results in,

$$\mathbf{G}^{\text{TE}}(\mathbf{r}, \mathbf{r}, \omega) = \int dq q \int_0^{2\pi} d\phi \mathbf{M}(\mathbf{q}, \mathbf{r}, \mathbf{r}) = \frac{i}{8\pi} \int dq \frac{q}{k_z} \begin{bmatrix} 1 & 0 & 0 \\ 0 & 1 & 0 \\ 0 & 0 & 0 \end{bmatrix} R_{\parallel}^{\text{TE}}(z), \quad (\text{E3})$$

and,

$$\mathbf{G}^{\text{TM}}(\mathbf{r}, \mathbf{r}, \omega) = \int dq q \int_0^{2\pi} d\phi \mathbf{N}(\mathbf{q}, \mathbf{r}, \mathbf{r}) = \frac{i}{8\pi k^2} \int dq \begin{bmatrix} q k_z R_{\parallel}^{\text{TM}}(z) & 0 & 0 \\ 0 & q k_z R_{\parallel}^{\text{TM}}(z) & 0 \\ 0 & 0 & 2q^3/k_z R_{\perp}^{\text{TM}}(z) \end{bmatrix} \quad (\text{E4})$$

Taking the emitter to be placed at  $z = 0$  and denoting the distance between the emitter and the top and bottom mirrors as  $t$  and  $b$  respectively, the reflection functions can be written as,

$$R_{\perp}^{\text{TM}}(z, q) = \frac{(1 + r_{cb}^{\text{TM}} e^{2ik_z b})(1 + r_{ct}^{\text{TM}} e^{2ik_z t})}{1 - r_{cb}^{\text{TM}} r_{ct}^{\text{TM}} e^{2ik_z d}} \quad (\text{E5})$$

$$R_{\parallel}^{\text{TE}}(z, q) = \frac{(1 + r_{cb}^{\text{TE}} e^{2ik_z b})(1 + r_{ct}^{\text{TE}} e^{2ik_z t})}{1 - r_{cb}^{\text{TE}} r_{ct}^{\text{TE}} e^{2ik_z d}} \quad (\text{E6})$$

$$R_{\parallel}^{\text{TM}}(z, q) = \frac{(1 - r_{cb}^{\text{TM}} e^{2ik_z b})(1 - r_{ct}^{\text{TM}} e^{2ik_z t})}{1 - r_{cb}^{\text{TM}} r_{ct}^{\text{TM}} e^{2ik_z d}} \quad (\text{E7})$$

The subscripts  $cb$  and  $ct$  refers to the interfaces between the cavity region and the bottom- and top mirror respectively. We use the following definition of the Fresnel coefficients for light incident on the interface between two regions  $a$  and  $b$  from region  $a$ ,

$$r_{ab}^{\text{TE}} = \frac{k_z^a - k_z^b}{k_z^a + k_z^b}, \quad (\text{E8})$$

$$r_{ab}^{\text{TM}} = \frac{\epsilon_b k_z^a - \epsilon_a k_z^b}{\epsilon_b k_z^a + \epsilon_a k_z^b}. \quad (\text{E9})$$

Note that these Fresnel coefficients could be replaced with the generalized Fresnel coefficients if more complicated mirrors such as e.g. distributed Bragg reflectors were considered.

### 1. Light-matter interaction in the Fabry-Perot cavity

Because the DGF is diagonal at  $\mathbf{r} = \mathbf{r}'$ , there is no coupling between the horizontal and vertical dipole orientations by feedback from the electromagnetic environment. Consequently, the local density of states (LDOS) for the two dipole orientations,

$$\rho(\mathbf{r}, \omega) = \frac{6\omega}{\pi c^2} \hat{n}_D \cdot \text{Im}[\mathbf{G}(\mathbf{r}, \mathbf{r}, \omega)] \cdot \hat{n}_D. \quad (\text{E10})$$

for a given dipole orientation  $\hat{n}_D$  becomes a direct proxy for the light-matter coupling strength. It can therefore be used to evaluate the potential of FPCs for realizing single/few emitter strong coupling. One concrete measure of the FPCs alterations of the electromagnetic environment is its modifications of the free space density of states. This is measured directly by the Purcell enhancement,

$$P_F(\mathbf{r}, \omega) = \frac{\rho(\mathbf{r}, \omega)}{\rho_0(\omega)}, \quad (\text{E11})$$

which is given as a rescaling of the LDOS by the free space density of states of the electromagnetic field,  $\rho_0(\omega)$ . To explore this, we consider two different FPCs, both of which consist of a central cavity region made of vacuum, surrounded by mirrors. In one instance, we consider idealized mirrors with a constant reflectivity of 0.95, and in the other we consider mirrors made of a Drude metal. In the latter case, we consider frequencies below the plasma frequency such that the mirrors retain their reflectivity. Supplementary Figure 2 shows the Purcell enhancement as a function of mirror distance,  $d$ , for a fixed emitter wavelength,  $\lambda_0$ , for idealized mirrors (b) and for Drude mirrors (c). In both cases, the horizontal and vertical dipole orientations are considered separately because, as mentioned above, the cavity does not couple the two.

Starting with Supplementary Figure 2 b) for the horizontal dipole orientation, we observe only relatively broad cavity resonances with modest Purcell enhancements of maximum  $\sim 2.5$ . This reflects the relatively weak concentration of the electromagnetic field in the FPC and emphasizes that the case with idealized mirrors is ill-suited for single point emitter strong coupling. We emphasize that the widths of these resonances are only weakly linked to the finite mirror reflectivity, and instead reflect the fact that the cavity features dispersion in plane. As such, these peaks would retain a finite width even in the limit of perfect mirror reflectivity [44]. For  $d < \lambda_0/2$  we observe a near complete suppression of the coupling of the horizontal dipole orientation to the electromagnetic environment. This happens because the horizontal dipole will always couple to the  $q = 0$  mode. This mode will not exist for  $d < \lambda_0/2$  with perfect mirrors and be strongly suppressed for near-perfect mirrors. This suppression can also be understood as a result of the mirror charge effect which will result in emission suppression for emitters with horizontal transition dipole moments when these are placed close to idealized reflective surfaces [17]. For the vertical dipole orientation, we generally observe relatively weak, near unity Purcell enhancement, except when  $d$  becomes smaller than  $\sim \lambda_0/2$ . From this point, the Purcell enhancement diverges as  $d \rightarrow 0$ . This divergence can be understood as a result of concentration of energy into the mode propagating parallel to the mirrors when the mirror distance is decreased [44]. Alternatively, it can also be more intuitively understood as a result of the mirror charge effect which enhances emission for vertical dipole orientations. For a single reflective interface, this enhancement would be a simple factor of 2 [17]. However, in the double mirror case, the image charge dipole in one mirror is enhanced by its mirror charge dipole in the second mirror and vice versa to infinity. Therefore, the Purcell enhancement diverges as  $d \rightarrow 0$  instead of approaching a simple factor of 2. When we consider the more realistic situation with mirrors described by the Drude model in Figure 2 c) we observe more or less the same as was the case with idealized mirrors. The only major difference is that we observe a divergence for the horizontal dipole orientation at small mirror distances. This happens due to near field coupling to the metal primarily representing quenching. We note that this also happens to the vertical dipole orientation but that this is less visible because of the mirror charge effect already causing a divergence like behaviour for  $d \rightarrow 0$  as was also the case with idealized mirrors.

The above discussion shows that the FPC provides only modest modification of the electromagnetic environment relative to the free space case with broad resonances whose width arise from the in-place dispersion of the cavity. The exception to this statement is for very small mirror spacing. However, in this latter regime the electromagnetic environment does not show resonant behaviour. For these reasons, we conclude that the FPC is ill-suited for single- and few emitter vacuum strong coupling. However, the FPC can still be suited for collective strong coupling [45] and coupling to extended systems [46] where the extended modes of the electromagnetic environment can be sampled more effectively.